Supplement of The Cryosphere, 20, 1867–1893, 2026
https://doi.org/10.5194/tc-20-1867-2026-supplement

The Cryosphere Open Access EGU

Supplement of

Past and future changes in avalanche problems in northern Norway estimated with machine-learning models

Kai-Uwe Eiselt and Rune Grand Graversen

Correspondence to: Kai-Uwe Eiselt (kai-uwe.eiselt@uit.no)

S1 Linear model for surface temperature

Here we describe the simple procedure we employ to obtain surface temperature values as input for the SNOWPACK simulations. We acquired three full years (1980, 1990, 2000) of hourly data for surface temperature (TS), 2 m temperature (T2m), 10 m wind speed (WS), and net long-wave (NLW) and short-wave (NSW) radiation from the ERA5 reanalysis archive. A representative ERA5 grid cell for the Troms county region was selected (several grid cells were tested, but the results exhibited little dependence on the exact location). The three-year timeseries data from this grid cell was split into training data (70 %) and test data (30 %). Fitting a linear regression model to the training data set we obtained the following model equation:

$$\mathrm{TSS} = -2.469 + 1.002 \times \mathrm{T2m} - 0.177 \times \mathrm{WS} + 5.499 \times 10^{-6} \times \mathrm{NSW} + 5.022 \times 10^{-6} \times \mathrm{NLW}, \tag{S1}$$

where the first value on the right-hand side represents the y intercept and the other values are the regression coefficients. It is clear that T2m has the largest impact and, as Fig. S1 shows, it is strongly correlated with both true and predicted TS. The linear model obtains an R^2 value of 0.97 and the root mean squared error for the three years is 3.93 K. The model thus gives a satisfactory representation of TS.

S2 Random forest model sensitivity analysis

Here we briefly present the sensitivity analysis conducted to assess the robustness of our conclusions based on the random forest (RF) model predictions. For this purpose we train three additional RF models with different avalanche seasons excluded as test data. We always exclude two avalanche seasons, being the winters ending in 2018 and 2022, 2019 and 2024, and 2020 and 2022. Recall that for the main RF model analysed in the study we excluded the winters ending in 2021 and 2023 (see section 3.1). In the following we first briefly analyse the quality of the RF model predictions and then compare the prediction results for the historical period and the future projections as presented in the study.

Figure S2 shows the true and predicted fraction of avalanche days (AvDs) for the different RF models. There is considerable variation in the model skill when it comes to reproducing the true fraction of AvDs, and some RF models overpredict the AvDs while others underpredict them. This may be related to the applied technique to balance the data (see section 3.2 on the SMOTE methodology). We have tested other class balancing methods but could not achieve an overall improvement of the RF model accuracy in predicting AvDs. More data are likely necessary to cover a larger range of possible instances and increase the RF model robustness.

Figure S3 shows the annual avalanche day frequency (ADF) for the general avalanche problem (AP) during the historical period (1970-2024) as predicted by the four different RF model as well as the linear trend slopes for the whole period. It is

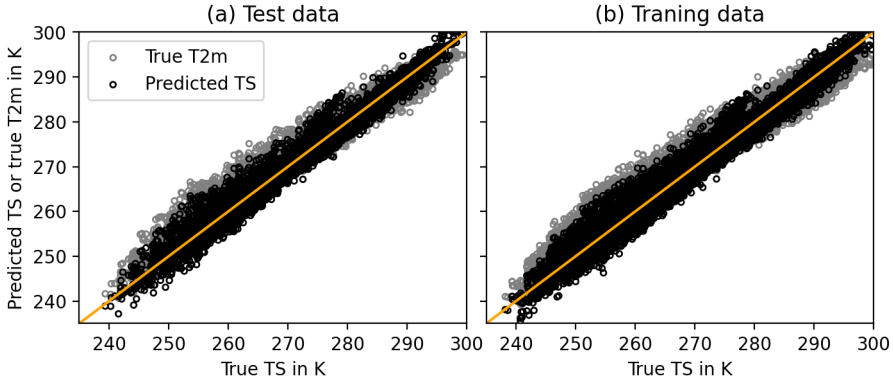

Figure S1. Relationship of the true and the predicted hourly ERA5 surface temperature (TS; black) for one grid cell in Troms county for (a) the test data and (b) the training data (see the text S1 for details). The grey dots represent the true values of the 2 m temperature (T2m). The orange line represents the 1:1 ratio. The linear model used to predict TS is given in eq. S1.

clear that while there is some variation, all four models exhibit mostly similar ADF values. Furthermore, all the linear trends over the historical period are small and not statistically significant. We note that for the other APs, there is more variation when it comes to the absolute ADF values, as can also be seen in Fig. S4 for the wind slab AP, but the results regarding the linear trends are consistent across all models (not shown). That is, the trends are small and in almost all cases statistically insignificant, confirming the conclusions in our study.

Figure S4 presents the 7 yr rolling mean ADF of the wind slab AP during the historical period as predicted by the four different RF models as well as the correlation coefficients (Pearson R) of the ADF with the Arctic Oscillation index. As indicated above, there is considerable variation when it comes to the absolute ADF values, but the evolution of the ADF over time is similar in all cases, and the ADF–AO correlation strong in almost all cases. The same is true for the wet and general APs and on the for annual values the corrlations are mostly statistically significant for these avalanche probelms (not shown), giving us confidence in the robustness of the conclusions in our study regarding the AO–ADF linkage.

Finally, S5 shows the ADF for the wet AP in the future climate projections for the four different RF models as well as the numerical changes between the historical and the late-century (LC) period. Again, as for the historical period, there is considerable variation of the absolute predicted ADF values across the RF model, but the development over time is mostly consistent. For the low-elevation regions (Tromsø and Sør-Troms) there is little change or a slight increase in the ADF towards the mid-century and then a strong decline towards the late century. The high-elevation regions (Nord-Troms, Lyngen, Indre Troms) exhibit either slight decline (Nord-Troms) or an increase (Lyngen, Indre Troms) in the mid-century and then a further increase (Nord-Troms, Indre Troms), or a constant ADF (Lyngen). There is considerable variation also in the strength of the changes in the ADF, but except for one case (Lyngen for the 2020/22 RF model; Fig. S5) they are statistically significant and qualitatively consistent. Thus, we are confident in the robustness of the conclusions in our study regarding the future development of avalanche problems in Troms.

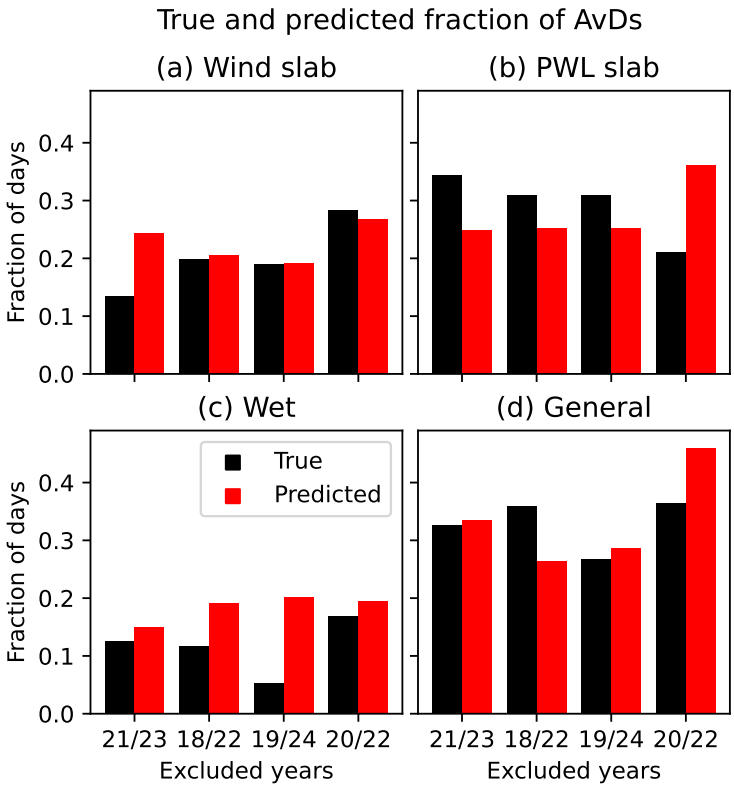

Figure S2. True (black) and predicted (red) fraction of avalanche days (AvDs) for the four different random forest models. The years excluded are indicated on the x axis (winters ending in 2021/23, 2018/22, 2019/24, 2020/22).

Table S1. Linear trends in d yr^{-1} of historical (NORA3) avalanche day frequency (ADF) for all avalanche problems (APs). Statistically significant trends ($p < 0.05$) are shown in bold type. The full season encompasses December through May, winter is December through February, and spring March through May.

	wind slab			PWL slab			wet			general		
	full	winter	spring	full	winter	spring	full	winter	spring	full	winter	spring
Nord-Troms	-0.06	-0.16	0.10	0.25	0.09	0.15	0.07	0.01	0.06	0.05	-0.08	0.13
Lyngen	0.01	-0.12	0.13	0.12	-0.02	0.13	0.03	0.03	0.00	0.11	-0.10	**0.21**
Tromsø	**-0.11**	-0.21	0.09	0.12	0.00	0.11	0.07	0.01	0.07	0.01	-0.18	**0.19**
Sør-Troms	-0.13	-0.18	0.05	0.03	-0.08	0.11	0.06	0.00	0.06	0.03	-0.12	0.15
Indre Troms	0.02	-0.08	0.09	0.26	0.15	0.11	0.11	0.03	0.08	0.13	-0.04	0.17

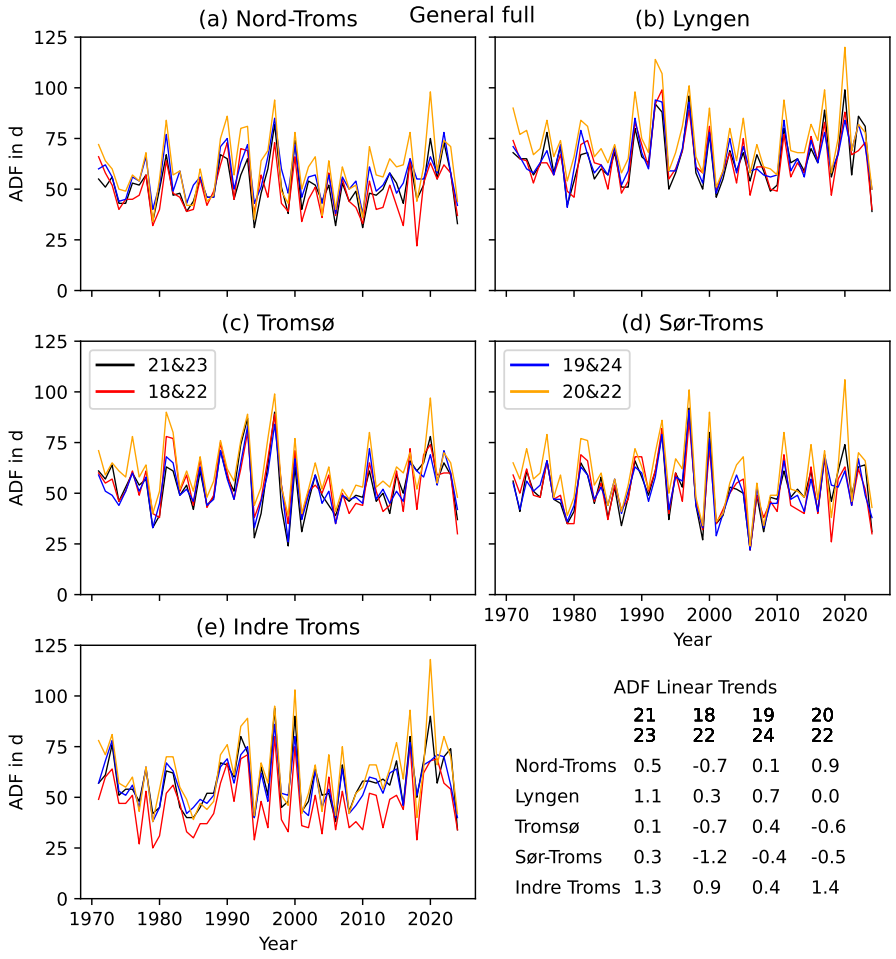

Figure S3. Annual avalanche-day frequency (ADF) for four different random forest models trained with different pairs of years (winters ending in 2021/23, 2018/22, 2019/24, 2020/24) excluded as test data. Shown is the general avalanche problem for the full season (Dec–May) for all warning regions. The numbers in the lower left panel represent the linear trend slopes in d dec^{-1}. Bold values indicate statistical significance at $p < 0.05$ (none present).

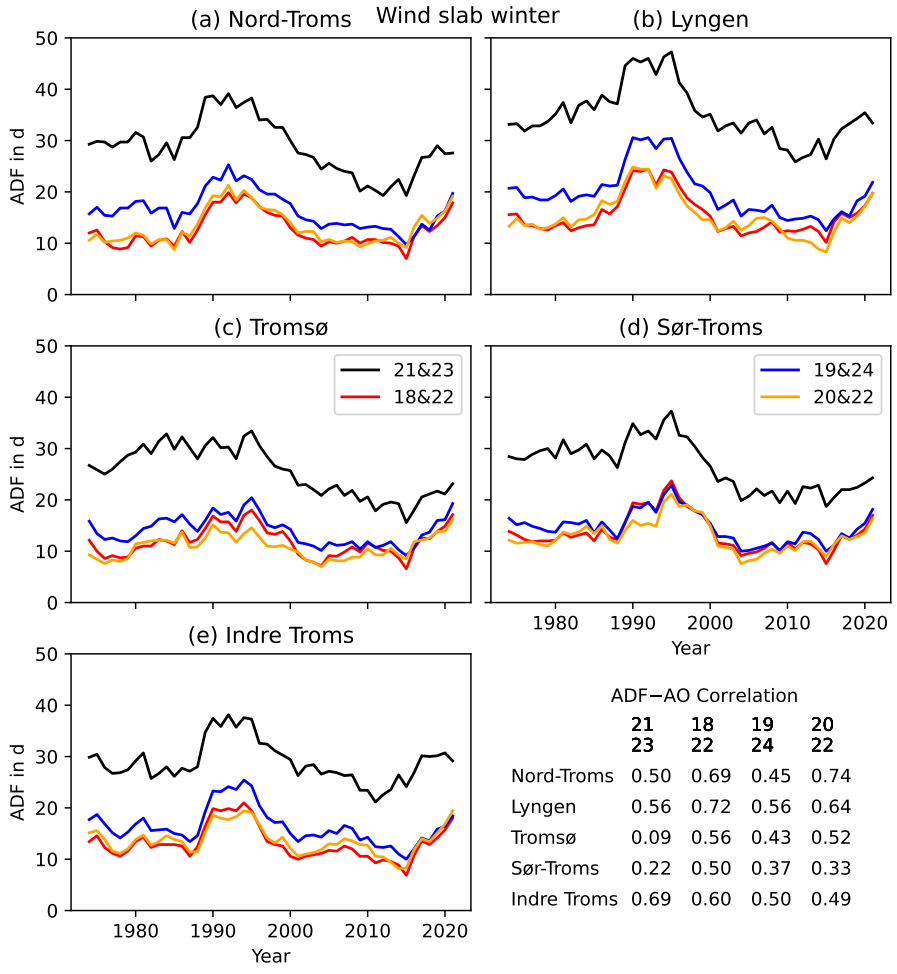

Figure S4. 7 yr rolling mean avalanche-day frequency (ADF) for four different random forest models trained with different pairs of years (winters ending in 2021/23, 2018/22, 2019/24, 2020/22) excluded as test data. Shown is the wind slab problem for the winter season (Dec–Feb) for all warning regions. The numbers in the lower left panel represent the correlation coefficient (Pearson R) of the ADF with the Arctic Oscillation index.

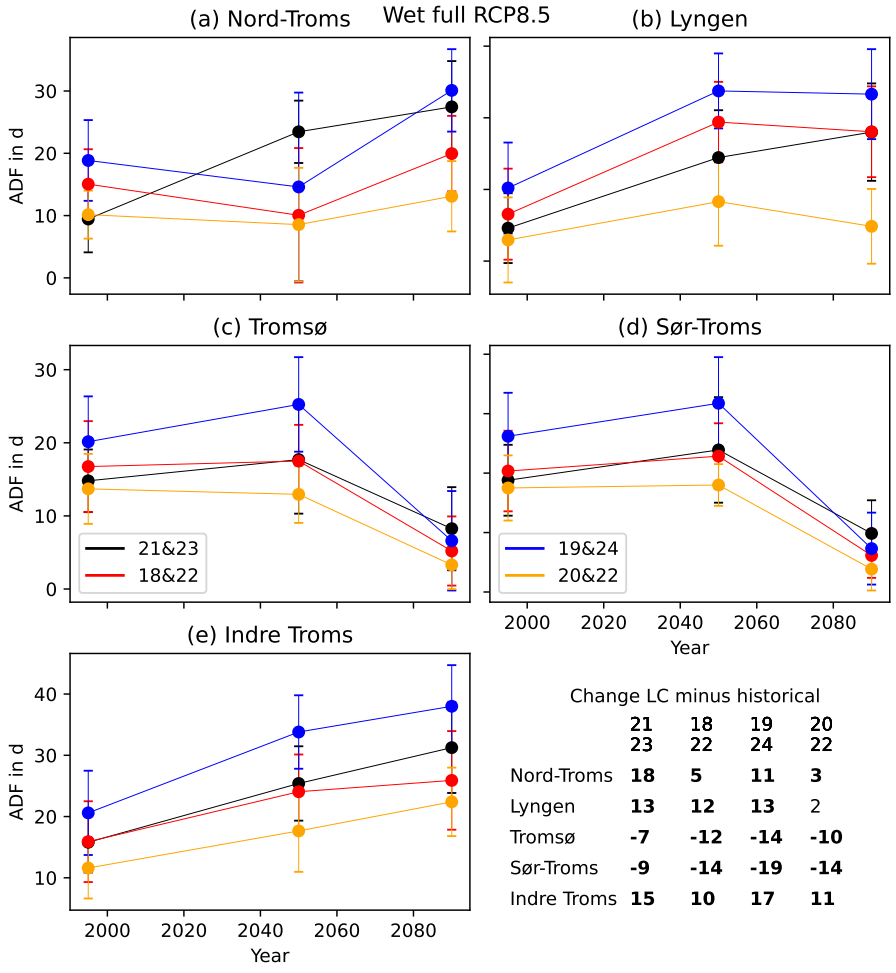

Figure S5. Historical (1985-2005), mid-century (2040-2060), and late-century (2080-2100) avalanche-day frequency (ADF) for four different random forest models trained with different pairs of years (winters ending in 2021/23, 2018/22, 2019/24, 2020/22) excluded as test data. Shown is the wet avalanche problem for the full season (Dec–May) for all warning regions. The errorbars indicate the standard deviations of the individual 20-year periods. The errorbars are slightly horizontally shifted for better readability. The numbers in the lower left panel represent the difference between the historical and the late-century values. Bold values indicate statistical significance at $p < 0.05$ based on a Monte-Carlo simulation with 100,000 permutations (see Appendix B).

Table S2. Correlation (Pearson R) of winter (Dec-Feb) avalanche day frequency (ADF) with Arctic Oscillation (AO) index. Statistically significant correlations ($p < 0.05$) for the 1 yr values are shown in bold type.

	wind slab		PWL slab		wet		general	
	1 yr	7 yr	1 yr	7 yr	1 yr	7 yr	1 yr	7 yr
Nord-Troms	**0.34**	0.50	-0.11	-0.22	**0.43**	0.75	**0.39**	0.55
Lyngen	**0.41**	0.56	-0.12	-0.27	**0.53**	0.83	**0.43**	0.60
Tromsø	0.22	0.09	-0.11	-0.56	**0.43**	0.72	**0.37**	0.42
Sør-Troms	**0.32**	0.22	**-0.31**	-0.73	**0.54**	0.73	**0.39**	0.51
Indre Troms	**0.49**	0.69	-0.18	-0.51	**0.44**	0.82	**0.47**	0.76

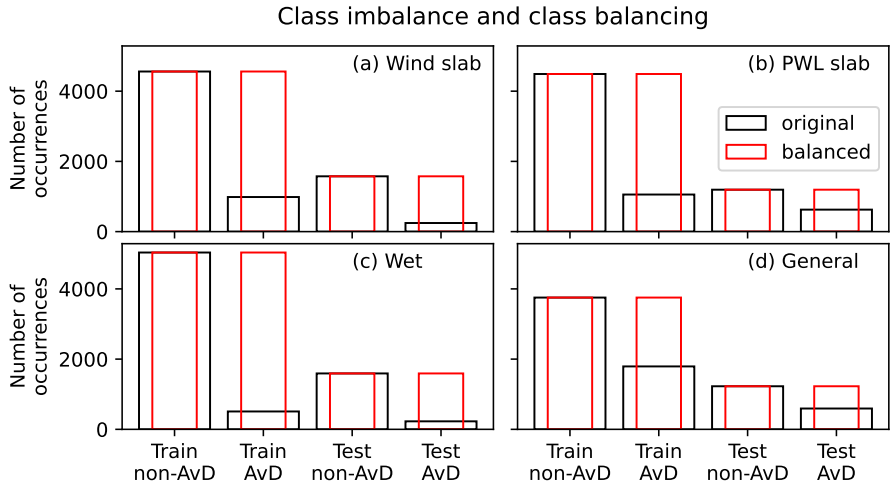

Figure S6. Class imbalance of training and test data. The number of avalanche days (AvDs) and non-avalanche days (non-AvDs) is shown for the original imbalanced data in black and for the balanced data in red. The balancing was performed with the SMOTE (see section 3.2).

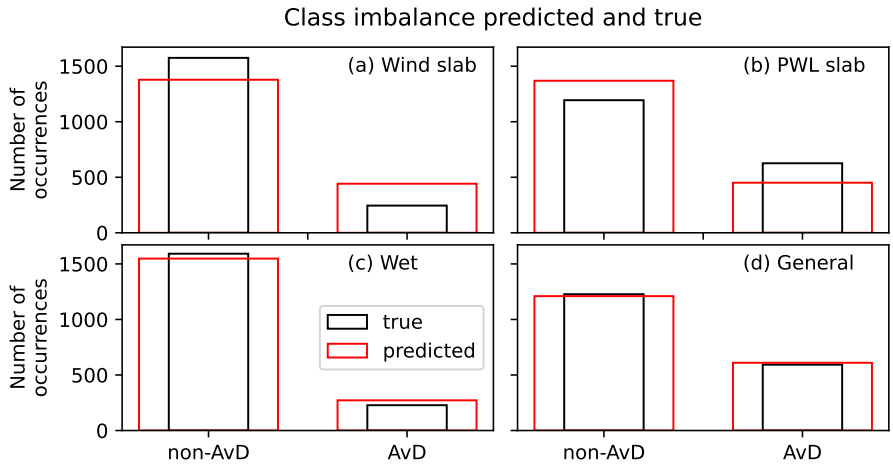

Figure S7. Class imbalance of true (black) and predicted (red) test data for non-avalanche days (non-AvDs) and avalanche days (AvDs) for the different avalanche problems.

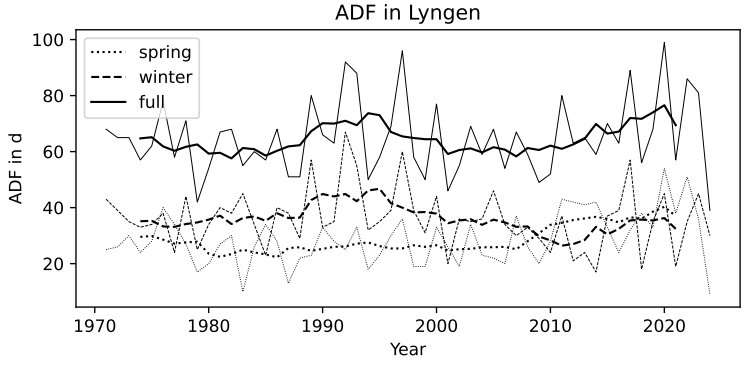

Figure S8. Historical (1970–2024) avalanche day frequency (ADF) in Lyngen for winter (dashed), spring (dotted), and full (solid) season. Thin and bold lines represent annual and 7 yr rolling mean values, respectively.

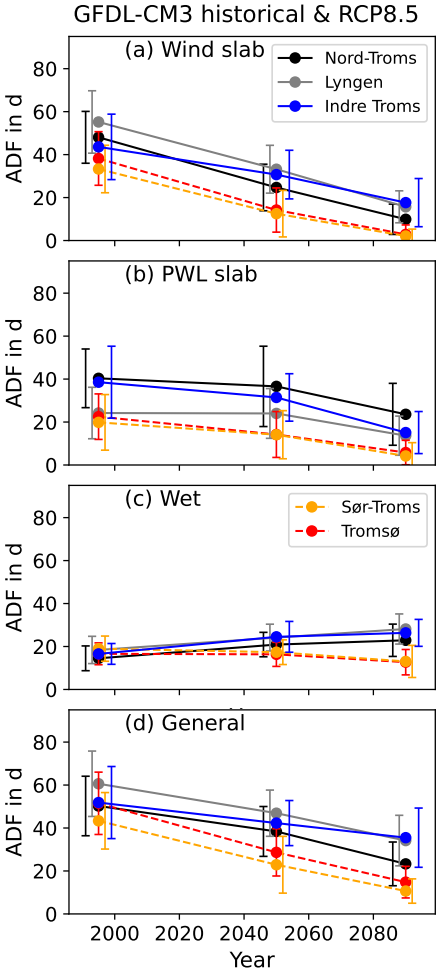

Figure S9. As Fig. 9 but for the GFDL-CM3. Only the RCP8.5 scenario is presented since RCP4.5 is not available for GFDL-CM3.

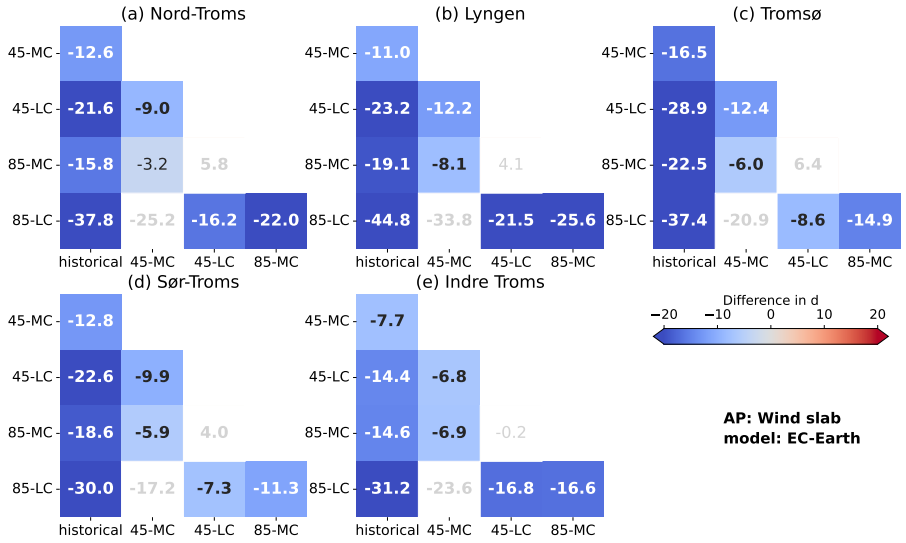

Figure S10. Changes of the wind slab avalanche day frequency (ADF) in the EC-Earth RCP4.5 and RCP8.5 simulations for the historical, mid-century (MC), and late-century (LC) periods. Bold values indicate significance on the $p < 0.05$ level based on a Monte-Carlo simulation with 100,000 permutations (see Appendix B). Changes are calculated as scenario on the y axis minus scenario on the x axis.

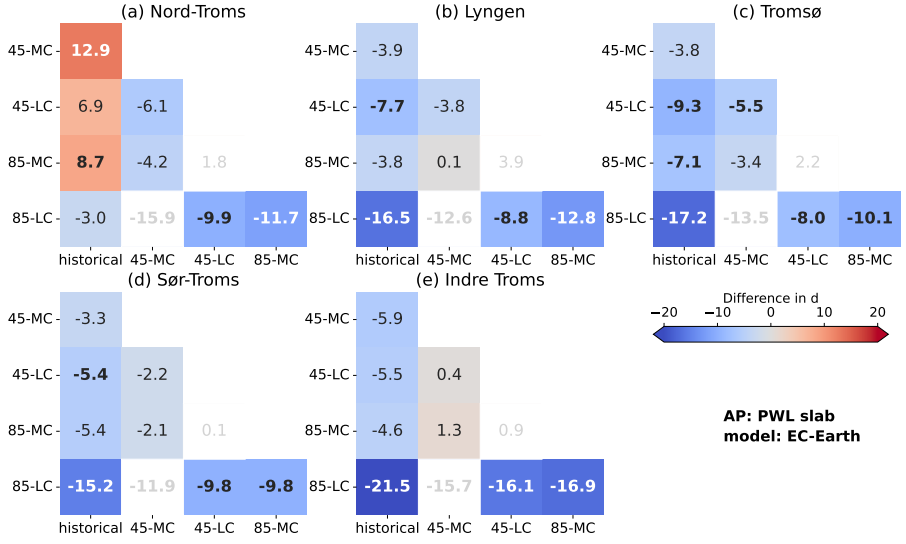

Figure S11. Same as Fig. S10 but for the PWL slab problem.

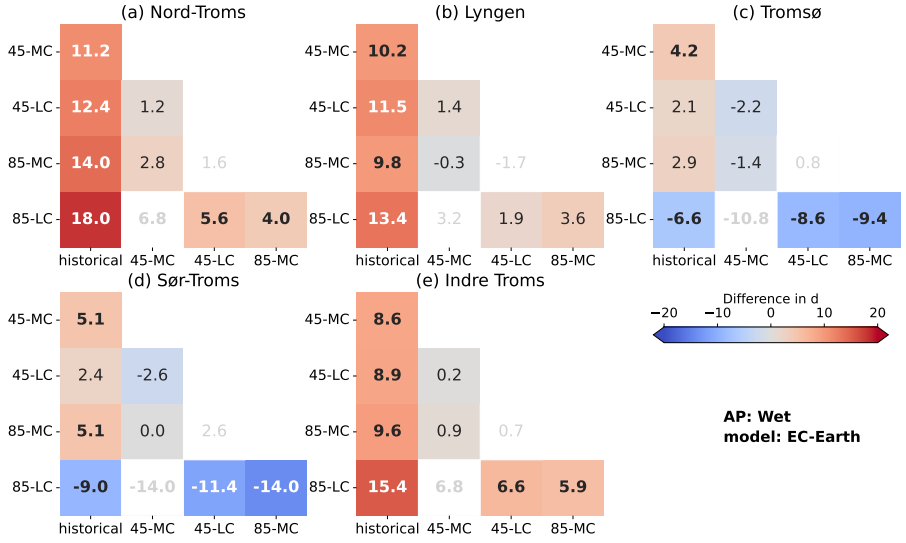

Figure S12. Same as Fig. S10 but for the wet problem.

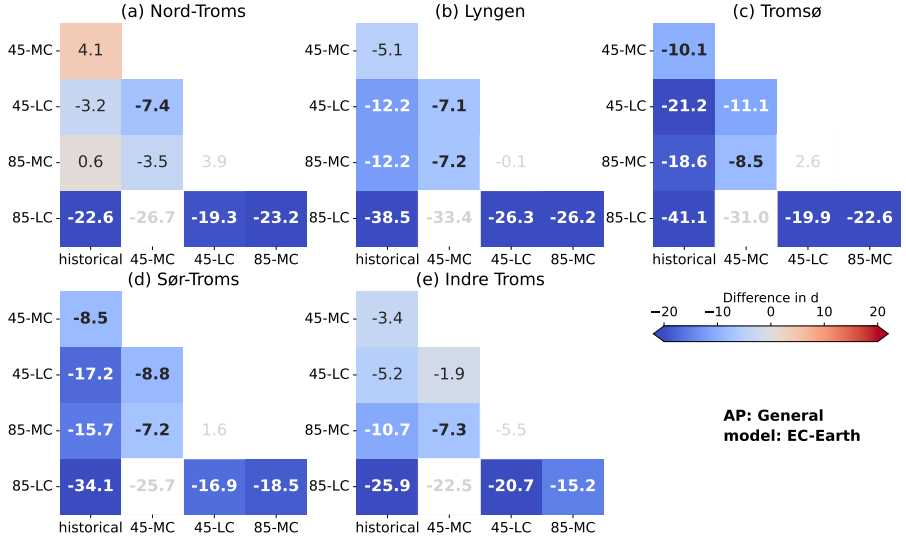

Figure S13. Same as Fig. S10 but for the general problem.

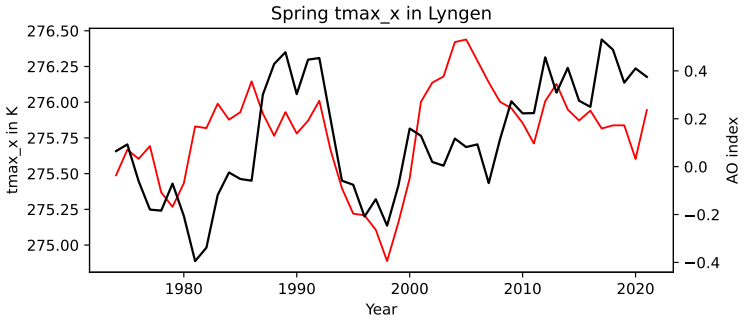

Figure S14. Spring average (Mar–May) of the maximum over all elevation bands of the daily maximum temperature (red; t_max_emax) and Arctic Oscillation (AO) index (black) in Lyngen for the historical period (1970–2024).

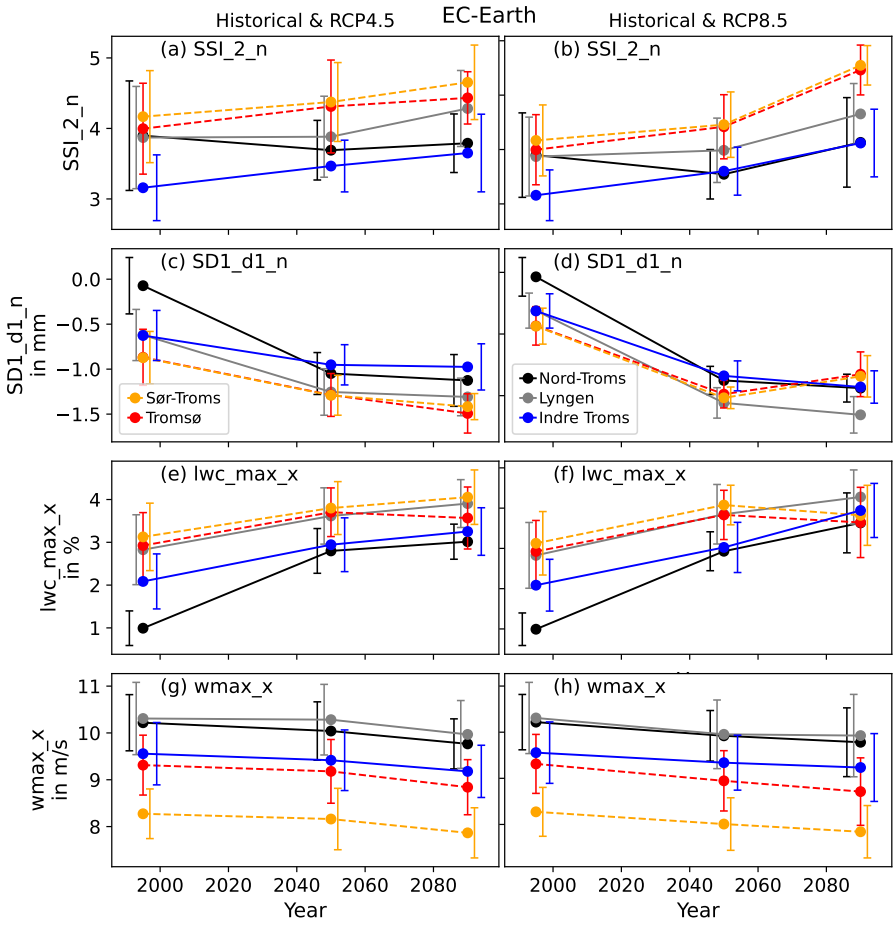

Figure S15. As Fig. 11 but for different features. Shown are the structural stability index at the second weak layer found in the snowpack (SSI_2; minimum across elevations), the one-day change of the snow depth (SD1_d1_n; minimum across elevations), the maximum liquid water content in the snowpack (lwc_max_x; maximum across elevations), and the daily maximum wind speed (wmax_x; maximum across elevations). See Tables C1 and C2 in Appendix C for more details.

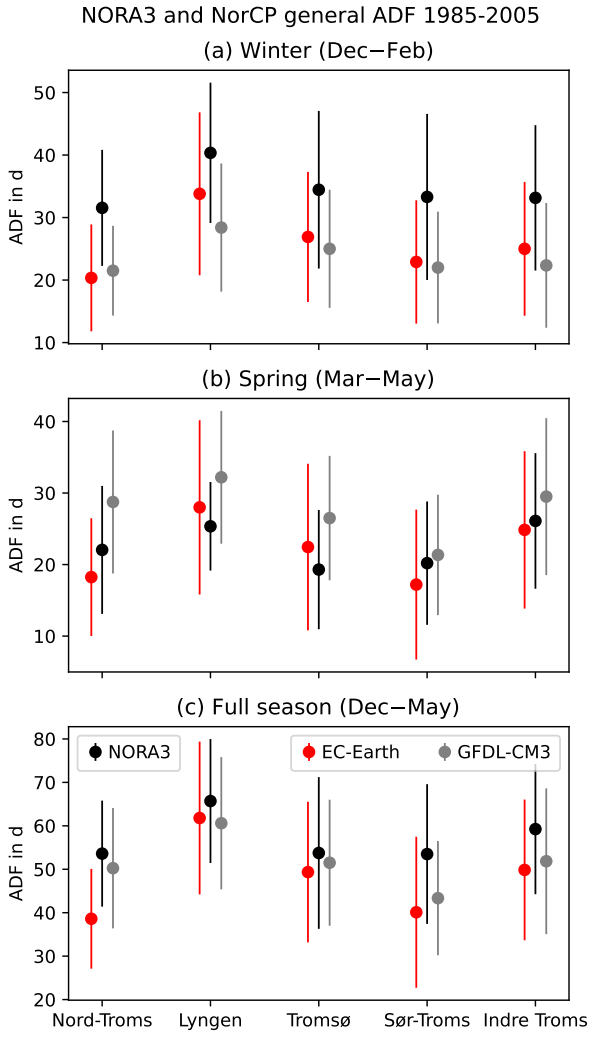

Figure S16. Historical (1985–2005) general avalanche-day frequency (ADF) for NORA3 (black), EC-Earth (red), and GFDL-CM3 (grey). Shown are (a) winter, (b) spring, and (c) the full avalanche season. The dots show the means over the 1985-2005 period for the individual avalanche regions and the errorbars indicate one standard deviation.

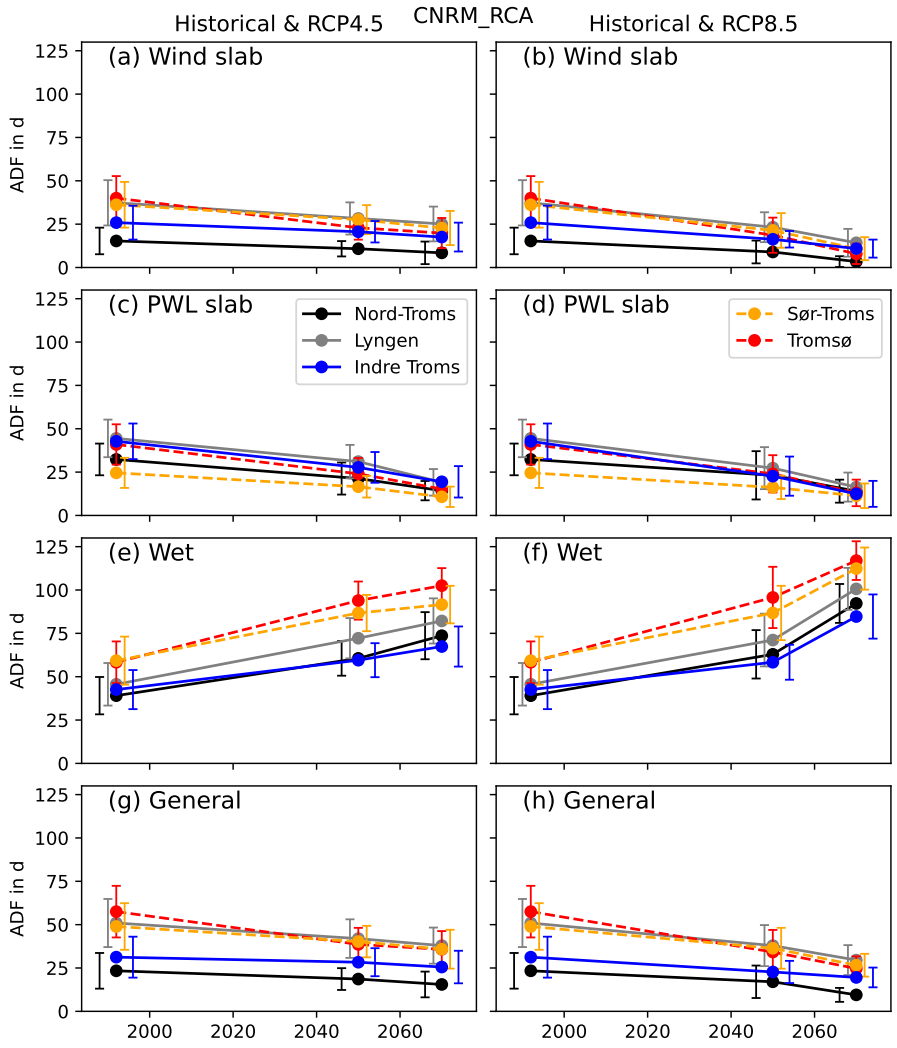

Figure S17. As Fig. 9 but for the statistically downscaled CNRM-RCA model from EURO-CORDEX. Note that for the statistically downscaled EURO-CORDEX data show a stronger warming response than the NorCP data. Interestingly, the latter show a cold bias in near-surface temperatures (Lind et al., 2020), while the former were bias-corrected to exhibit higher temperatures (Wong et al., 2016).

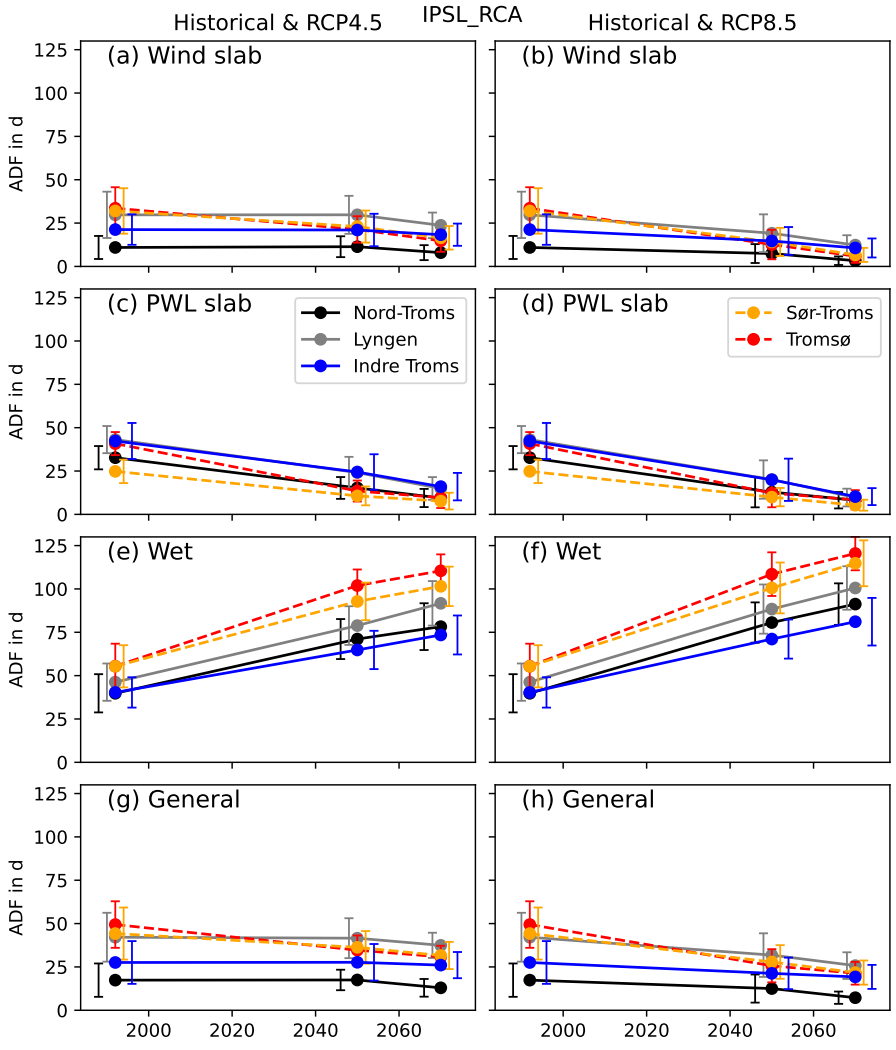

Figure S18. As Fig. 9 but for the statistically downscaled IPSL-RCA model from EURO-CORDEX.

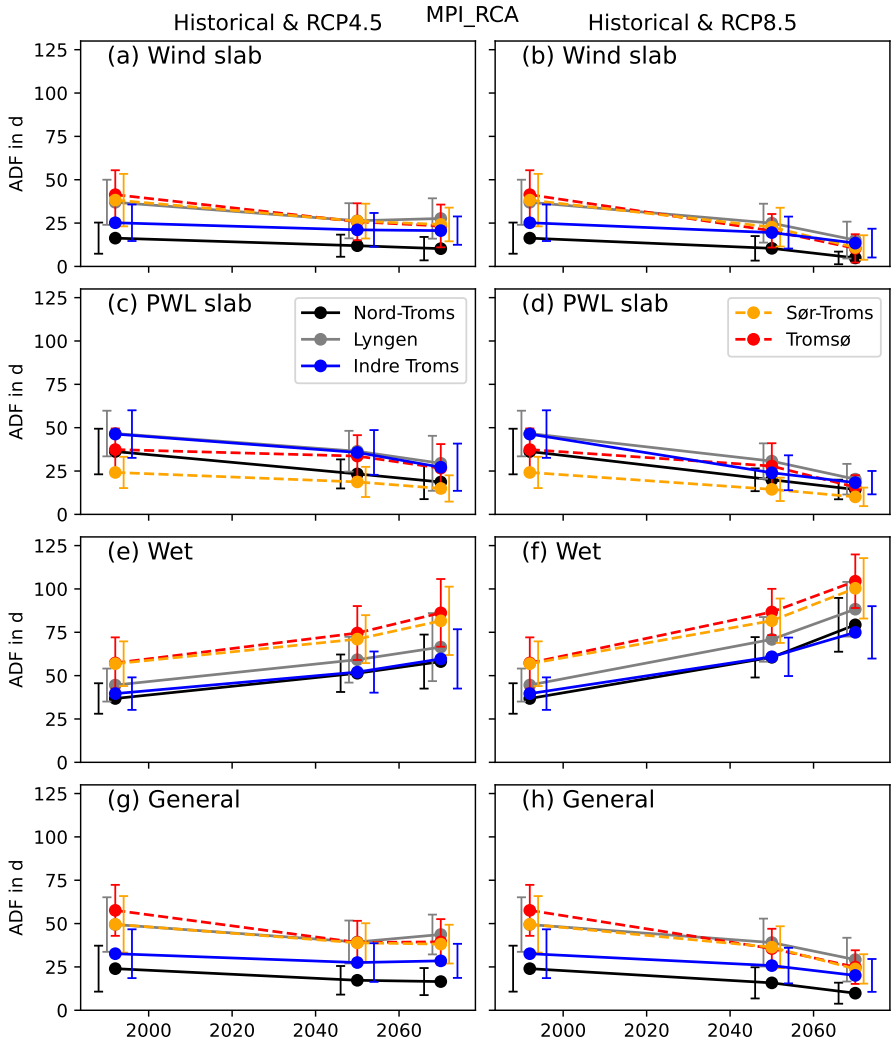

Figure S19. As Fig. 9 but for the statistically downscaled MPI-RCA model from EURO-CORDEX.

References

Lind, P., Belušić, D., Christensen, O. B., Dobler, A., Kjellström, E., Landgren, O., Lindstedt, D., Matte, D., Pedersen, R. A., Toivonen, E., and Wang, F.: Benefits and added value of convection-permitting climate modeling over Fenno-Scandinavia, Climate Dyn., 55, 1893–1912, https://doi.org/10.1007/s00382-020-05359-3, 2020.

Wong, W. K., Haddeland, I., Lawrence, D., and Beldring, S.: Gridded 1×1 km Climate and Hydrological Projections for Norway, NVE Report 59–2016, Norwegian Water Resources and Energy Directorate, https://nve.brage.unit.no/nve-xmlui/handle/11250/2500569, 2016.